Langmuir

Article

pubs.acs.org/Langmuir

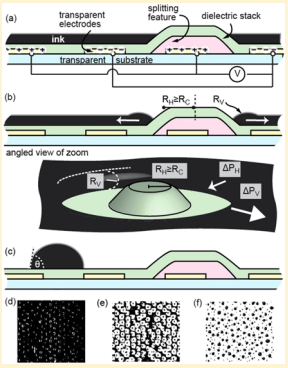
Scaling Dielectrowetting Optical Shutters to Higher Resolution: Microfluidic and Optical Implications

A. Russell, E. Kreit, and J. Heikenfeld*

Novel Device Laboratory, School of Electrical Engineering and Computing Systems, University of Cincinnati, Cincinnati, Ohio 45221, United States

Supporting Information

ABSTRACT: A detailed study is reported on the implications of scaling dielectrowetting optical shutters to higher resolutions. Reducing droplet sizes from millimeters to 100 μm in diameter increases the relevance of microfluidic physics such as pinning, film breakup, and dewetting speed as well as optical physics such as transmission and diffraction. In addition, in this work we present improved material systems, including optimized dielectric stacks which reduce electrochemical degradation, and blended lower-viscosity fluids which increase dewetting speed. A higher-resolution device of ~250 μm diameter demonstrates switching speeds of <100 ms and a clear, optically transmissive aperture of >70%. In addition to revealing science not previously discussed, this work has strong applied importance as scaling to higher resolutions is desirable for improving visual appearance in applications ranging from smart windows to electronic signage.



Downloaded via UNIV OF CINCINNATI on August 19, 2018 at 19:47:09 (UTC).
See https://pubs.acs.org/sharingguidelines for options on how to legitimately share published articles.

INTRODUCTION

The size of electro-optic devices has reached an impressive scale, considering the commercial availability of liquid crystal displays with diagonals close to 100 inches. However, large-area applications such as smart windows[1] and reflective signage[2] remain underserved, as current technologies struggle to provide attributes such as glasslike optical transparency and low cost. Major technologies in commercial use for smart windows include electrochromic (EC),[3−5] polymer-dispersed liquid crystals (PDLCs),[6] and suspended particle devices (SPDs).[7]

Recently, we reported a novel dielectrowetting optical shutter which can provide a >80% optical aperture for transmission and is simple to construct in that it requires no alignment or pixelation of device features.[8] Here we report a detailed study on the implications of scaling dielectrowetting optical shutters to higher resolutions. In addition to being important from an applied perspective with faster switching and less visible droplets, this scaling reveals a fundamental understanding of the finer device physics and performance limits. For example, reducing droplet sizes from millimeters to 100 μm in diameter increases the relevance of microfluidic physics such as pinning, film breakup, and dewetting speed as well as optical physics such as transmission and diffraction. In addition, in this work we present improved material systems, including optimized dielectric stacks which reduce electrochemical degradation and blended lower-viscosity fluids which increase the dewetting speed. A higher-resolution device, with an ~250-μm-diameter droplet radius after dewetting, demonstrates switching speeds of <100 ms and an optically clear aperture of >70%. In addition to the applied value of this work and the increased theoretical understanding of dielectrowettting optical shutters, the findings may aid the investigation of scaling of similar microfluidic technologies.

DEVICE CONSTRUCTION AND THEORY: DEVICE FABRICATION AND OPERATION

Figure 1 shows an operating diagram and magnified photographs of the dielectrowetting optical shutter. The demonstrated fabrication process is simple and requires no photolithography, feature alignment, or pixelation. Aluminosilicate glass coated with indium tin oxide (100 Ω/cm) was purchased from Precision Glass & Optics and patterned with 40 μm interdigitated electrodes via laser ablation (Laserod Inc.). The electrodes were interdigitated with a 40 μm line width and gap spacing. Hexagonal arrays of splitting features were applied to the substrate and electrodes using a Diamatix printer and Magenta UV-curable polymer (Collins Ink). Carbon black or other partially conductive polymer dispersions were explicitly not used to prevent the electrical shorting of electrodes (only dye colorants were used). The splitting features were then UV cured with i-line-filtered (365 nm) light for 30 s at 5 mJ/cm^2 and baked 10 min at 180 °C. The substrate was then coated with 500 nm of vapor-deposited Parylene C (Specialty Coating Systems 2010). The Parylene was then dip coated with Cytonix FluoroPel 1601 V and baked in air for 30 min at 180 °C to form a uniform, ~50-nm-thick, and ~16 mN/m hydrophobic fluoropolymer layer. This dielectric stack halts the electrochemical attack of the electrodes yet is still thin enough that omnidirectional superspreading occurs (e.g., wetting across

Received: March 6, 2014
Revised: April 9, 2014
Published: April 15, 2014

 © 2014 American Chemical Society dx.doi.org/10.1021/la5008582 | Langmuir 2014, 30, 5357−5362

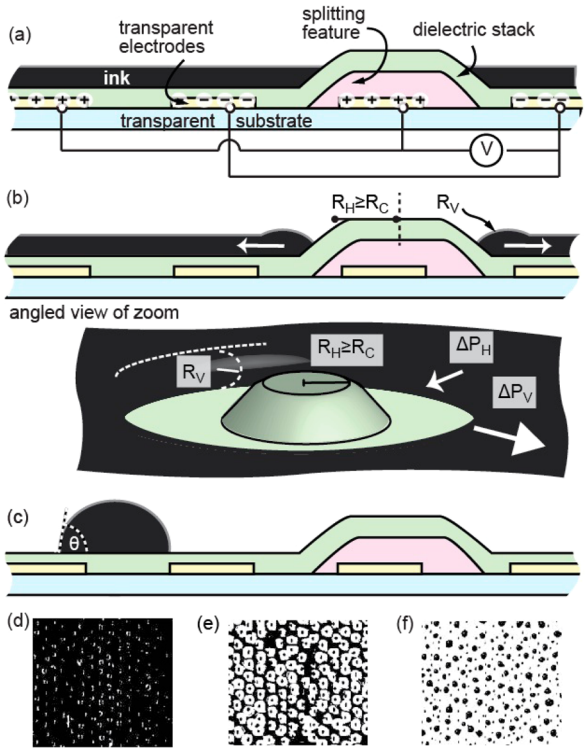


Figure 1. (a) Optical shutter in the on state, viewed as a diagram from the side and (d) top-view device photograph. (b) The splitting feature radius R_H must be greater than the critical radius R_C to nucleate fluid splitting properly. Looking at the angled view below, we see that ΔP_H hinders dewetting. ΔP_V promotes nucleated dewetting, as also seen in the top view (e). (c) Side-view diagram of the optical shutter in the off state and (f) the device as viewed from above.

electrodes also, more than just wetting along the electrodes where the dielectrophoretic force is strongest). Similar to our previous work,[8] square wave voltages of 110 V_p and 50 Hz were utilized in all device actuation tests. The dielectrowetting fluid was a proprietary liquid crystal (DIC Corp., Japan) chosen because of its very high electrical insulation and dielectric constant of $\varepsilon \approx 35$. The liquid crystal fluid was colored blue with 1.0 wt % Keystone Analine Corp. liquid oil blue dye (USA). For this work, the blue dye was highly purified of electrically conductive contaminants by Unichem Corp. (Taiwan). The fluid surface tension was $\gamma \approx 39$ mN m^{-1}, and on the fluoropolymer, the fluid has a Young's angle of $\theta \approx 85°$. This liquid crystal/dye is the dielectrowetted fluid and is herein referred to as the ink.

Regarding the dielectrowetting operation, when voltage is applied, nonuniform electric fields generated by the interdigitated electrodes exert a dielectrophoretic force (F) on ink droplets. The applied dielectrophoretic force follows a V^2 relationship similar to that for electrowetting[9−11] but unlike electrowetting is able to reduce the contact angle of the ink droplet to zero (superspreading).[12,13] In the superspread state, the opaque ink film blocks incident light and results in a black appearance as shown in Figure 1(a,d). Black coloring of the polymer splitting feature results in the absorption of light over the majority of the device area ($\%T < 1.5\%$,[8]).

Regarding dewetting after the voltage is removed, van der Waals forces are entirely too small for the localized and spontaneous breakup of the ∼10-μm-thick ink film.[14] Splitting features (Figure 1(b,e)) were therefore used for the deterministic breakup of the ink film, having a thickness of 12−15 μm and $\varepsilon = 3.61$ such that they have lower electrical capacitance than the ink film such that the ink film does not superspread over the splitting features. This promotes nucleated dewetting when voltage is removed from the splitting features and results in faster dewetting times and smaller droplets which are not affected by gravity[8] (Figure 1(c,f)). The alternative to splitting features would be to utilize pixelation,[15] which increases fabrication complexity and reduces the clear optical aperture.

The ink requires a minimum size splitting feature R_C to nucleate dewetting[14] (Figure 1(b,e)), which for an unstable film thickness and contact angle a first-order approximation is

$$R_c = \frac{h}{\tan\theta(\sqrt{(1+\cos\theta)} - 1)} \quad (1)$$

Using the value $h = 10$ μm for the thickness of the ink film and $\theta < 10-90°$ for contact angle predicts $R_C \gtrsim 135$ to 20 μm. If ink splitting is attempted with a "hole" in the ink that is less than R_C, then the horizontal component of Laplace pressure R_H (Figure 1(b)), which hinders dewetting, will instead cause the ink to remain wetted around the splitting feature[16,17] according to

$$P_L = \frac{2_{\gamma LV}}{R_V + R_H} \quad (2)$$

where P_L is the Laplace pressure, γ_{LV} is the liquid−vapor surface tension, R_V is the positive vertical radius of curvature, and R_H is the negative horizontal radius of curvature of the fluid. If the splitting feature is greater than R_C, then the pressure of dewetting ΔP_V will override ΔP_H and the ink will dewet from the splitting feature. A range of angles and R_C are given because the contact angle is dynamic when voltage is first removed, and exact calculation is therefore more complicated.

PHYSICS OF DEVICE SCALING

Scaling and Microfluidic Effects. In this section, three finer microfluidic effects are discussed. First, the previous section discussed the need for a minimum radius for the splitting features, $R_H > R_C$. Creating smaller splitting features would benefit optical transmission as the pitch of the splitting features is scaled to smaller sizes. However, in this section, it is shown that the side-wall slope of the splitting features must also be carefully designed. Second, the effects of fluid viscosity are discussed, with the specific purpose of increasing the dewetting speed of the device. Third, the dewetting speed of the device can be increased if the ink has to travel less distance to dewet, achievable by having more closely spaced splitting features but having a limit as ink starts to pin between splitting features as a new horizontal component to the Laplace pressure emerges.

Microfluidic pinning (sticking) around the splitting features can prevent deterministic dewetting in extreme cases and even as dewetting occurs can cause droplets to stick to splitting features, reducing the switching speed and optical transmission. Pinning is a result of geometry and hydrophobicity in this work, and maximally hydrophobic materials are already utilized. Textured "superhydrophobic" surfaces are not an option because during dielectrowetting they would be irreversibly wetted into the Wenzel state.[18] The only alternative is, therefore, to modify the side-wall angle of the splitting feature as shown in Figure 2. Several side-wall angles are now examined. First, consider splitting features with vertical side

dx.doi.org/10.1021/la5008582 | Langmuir 2014, 30, 5357−5362

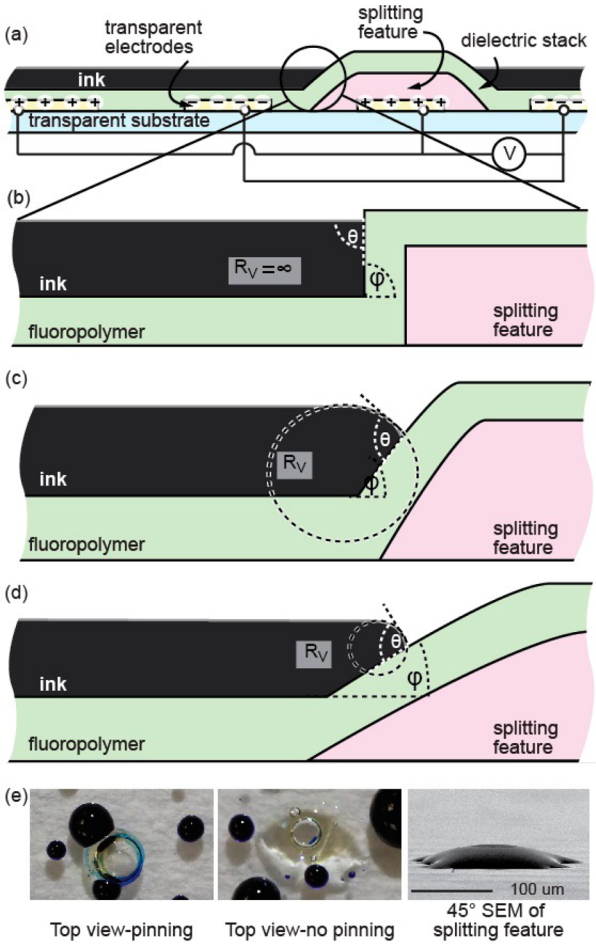


Figure 2. (a) Diagram of sloped splitting feature device. (b) $\varphi = 90°$ results in pinning and infinitely large R_V. (c,d) R_V is decreasing with smaller φ, and dewetting occurs as $\Delta P_V \gg \Delta P_H$. (e) Photographs: (left) $\varphi \approx 85°$ angle, pinning occurs on the splitting feature corner, (middle) top view of no pinning, $\varphi \approx 50°$, (right) example SEM of the sloped sidewall splitting feature used in device fabrication.

walls (Figure 2b); for a Young's angle (θ) near 90° and with $\varphi = 90°$, an infinite R_V could exist and therefore no ΔP_V would exist to enable deterministic dewetting. For $\varphi > 90°$, the problem would be worse, and R_V and ΔP_V would invert and pull ink into the corner of the splitting feature. For these reasons, conventional photolithography was not utilized to create splitting features, and techniques for creating splitting features with sloped sidewalls were instead utilized.

The inkjet printing method used produces a splitting feature with a $\varphi \approx 50°$ side-wall angle as shown in the right-most photograph of Figure 2e. For sloped side walls, as shown in the diagrams of Figure 2(c,d), R_V has decreased, resulting in larger ΔP_V (creating dewetting pressure, eliminating pinning). Further photographs in Figure 2e are for pinned and no-pinned cases, similar to Figure 2(b,c), respectively. In the pinned photograph, one can even observe a ring of ink trapped along the perimeter of the splitting feature. An attempt was made to develop a theoretical model which predicted ΔP_V as a function of h, φ, and θ, but in experimental observations it was clear that hysteresis and dynamic (nonequilibrium) meniscus profiles would make such a theoretical model a gross approximation at best. Regardless, it can be concluded that sloped splitting features are essential for a proper deterministic dewetting of the ink film. Additionally, as splitting features are made smaller and ΔP_H increases, at some point side-wall angle φ must continue to be reduced to promote ink dewetting. The limit (albeit impractical) would be $\varphi = 0°$, at which R_V would be equal to h for a 90° ink contact angle; therefore, $R_H > h$. However, $\varphi \gg 0°$ is required to maintain the lower electrical capacitance provided by the splitting features which prevents dielectrowetting superspreading over the top splitting features.

Optimization of speed through reduced ink viscosity was sought as well. Zhao[8] showed the dewetting speed to be more than double that of wetting. Therefore, the focus here is on reducing the dewetting time, which unlike the wetting time can be resolved only through microfluidic design, not through dielectrowetting improvements. The distance between splitting features (splitting feature pitch) determines the subsequent droplet radius,[16] and smaller and more closely spaced droplets result in a faster dewetting/wetting speed by simply reducing the distance the ink has to travel. A significant reduction in dewetting time by scaling down the splitting feature pitch is experimentally shown in Figure 3.[8] It can be seen that as the feature pitch decreases from 3.5 to 0.85 mm, the dewetting time drops from 750 to 300 ms. A further decrease in the pitch of the splitting features was not sought because, as will be discussed in the next paragraph, another form of ink pinning becomes problematic for very small pitches of splitting features. Therefore, to reduce the dewetting time further, the alternate approach of reducing the ink viscosity was used.[19] The ink viscosity was reduced by blending with a high-dielectric constant, insulating nitrobenzene ($\varepsilon = 34.8$) in a 4:1 ratio (Sigma-Aldrich, ≥99.0% purity). The nitrobenzene viscosity is 1.8 cP, much lower than the liquid crystal viscosity at ~50 cP. The nitrobenzene blend further improves the dewetting speed to ~75 ms, a 4-fold decrease. Nitrobenzene was specifically chosen because a high dielectric constant for the ink must be maintained to minimize the operating voltage.

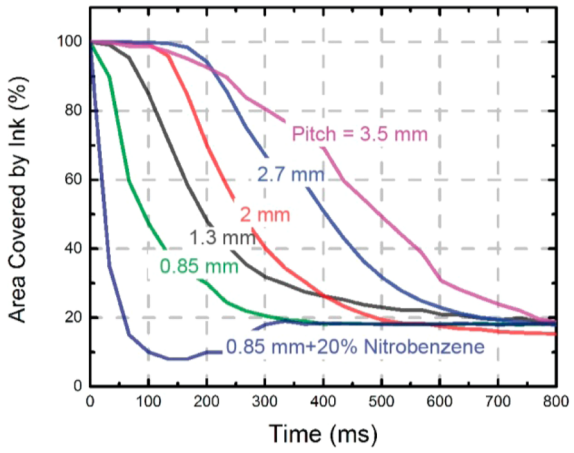


Figure 3. Switching speeds of various splitting feature pitches ranging from 3.5 to 0.85 mm using liquid crystal ink. A corresponding decrease is observed as the switching speed drops from 750 to 300 ms. The fastest switching speed (~75 ms) is seen using a 20% nitrobenzene and 80% liquid crystal blend with a 0.85 mm pitch.

As previously shown and discussed for Figure 3, a reducing splitting feature pitch improves the dewetting speed, but another limiting factor unfortunately appears. For advancing ink wetting in between splitting features, where wetting is also partly governed by Laplace, there is another horizontally

dx.doi.org/10.1021/la5008582 | Langmuir 2014, 30, 5357−5362

derived Laplace pressure that is positive and can therefore limit ink spreading.[20,21] As shown in Figure 4, this new convex

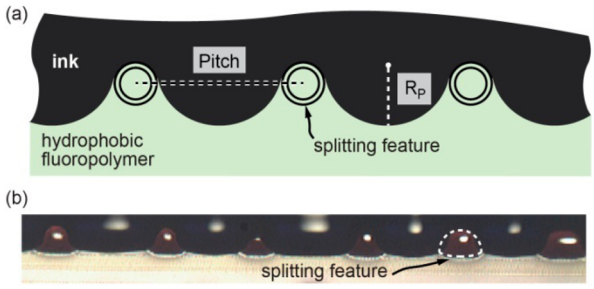


Figure 4. (a) Diagram top view: pinning between features occurs when $\Delta P_H \leq \Delta P_V$. When the distance between the splitting features increases and $R_H < R_V$ (and thus $\Delta P_H > \Delta P_V$), the ink sheet now has adequate horizontal Laplace pressure to wet through the row of splitting features. (b) A side view of a splitting feature.

horizontal radius of curvature causing pinning (R_P) and becomes significant as the pitch between splitting features is decreased ($R_P \approx$ pitch/2). Experimentally, pinning became significant and problematic for a pitch of 0.75 mm, which is why further reductions in pitch were not sought for the data in Figure 3. For the materials and layer thicknesses utilized in this report, a splitting feature pitch of ≥0.85 mm was generally observed to operate reliably without pinning between splitting features.

Scaling and Optical Effects. In this section, three optical effects are discussed which significantly impact applications such as windows and signage. First, the transmissivity of the device versus droplet radius is discussed, which flows from previous sections where the splitting feature pitch was shown to control the dewetted droplet radius. Second, the device plane is highly optically inhomogeneous, with both periodic arrangements of electrodes and splitting features, giving rise to optical diffraction and thus reducing the visible optical clarity of the device. Lastly, it is recognized that the splitting feature pitch can be varied in a single device, and the dynamics of dewetting can be used to impart perceived motion or other visible effects.

The optical transmissivity was investigated both theoretically and experimentally as a function of the dewetted droplet radius. For a sheet of ink with a given finite volume, the area versus volume ratio of individual droplets causes transparency to fall as droplets become smaller and cover more area per unit volume, according to the relationship

$$V = \frac{\pi D_{cap}^{\ 3}}{24 \sin^3 \theta}(1 - \cos\theta)^2(2 + \cos\theta) \quad (3)$$

where V is volume, D is the diameter of the droplet spherical cap, and θ is the Young's angle.[22] The theoretical plot of this relationship can be seen in Figure 5. The experimental data in Figure 5 were for a droplet radius range of 987 to 510 μm, created by splitting feature pitches ranging from 0.85 to 3.5 mm.

As the droplet radius decreases, the number of droplets per cm^2 increases, an intuitive result. As the number of droplets per area increases, transmission decreases—the same volume now takes up more area in the voltage-off state. This was verified experimentally; looking at Figure 5 it can be seen that as the droplet radius decreases, the droplet number per cm^2 increases while transmission falls. The limited range in the experimental

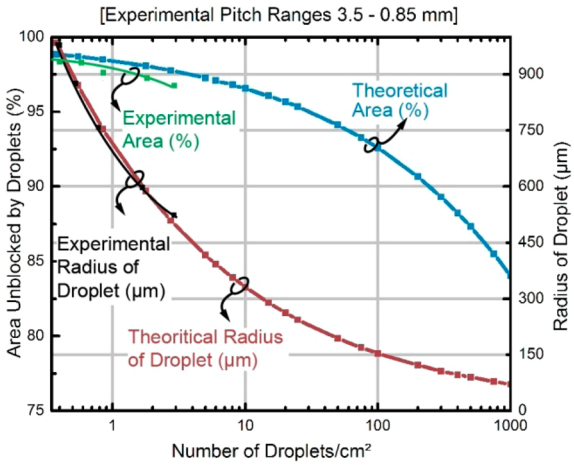


Figure 5. Theoretical calculation of droplet radii versus transmissive area and resulting number of droplets per cm^2. As the droplets decrease in radius, the number of droplets increases. More droplets result in less transmission, which was also observed experimentally.

data is the same limit described in the previous section (pitch limit, pinning between features). It is important to note that the reflection of the patterned ITO and glass substrate has been removed from the data of Figure 5, which shows the percent transmissive area (not the total percent transmission). The data for the area not covered by ink does not include the area occupied by the splitting features, which, however, is negligible compared to that of the dewetted droplets.

Outside of the ink and the splitting features, the entire device is composed of transparent materials. Except for the ITO electrodes, transparent materials are homogeneously coated as thin films, causing at worse a transmission color shift due to optical thin film interference. The splitting features are opaque; therefore, their "lenslet" shape does not cause significant refraction (scattering of light). However, optical diffraction is not resolved by the transmission of the ITO electrodes nor the opacity of the splitting features because both features have a significant periodicity in the geometrical arrangement. The 50-nm-thick, 40-μm-wide, patterned ITO electrodes were not index matched to the glass substrate or the films coated above them, resulting in significant optical diffraction as shown in Figure 6a. The analysis in Figure 6 includes (left) a photograph of the diffracting features, (middle) a 2D discrete Fourier transform (FT),[23,24] and (right) a photograph of a 7 mm spot size, 650 nm laser, 5 m from the laser and photographs taken 10 cm after the sample on a white target. Custom code for the Fourier analysis was written and is included as online Supporting Information for this report. For the ITO electrodes (Figure 6a), agreement is obviously visible between the Fourier transform and the photographs of the laser diffraction. This identifies a clear need to replace ITO in applications where visible clarity is critical. Because we have developed very low frequency electrical operation[8] for dielectrowetting superspreading (1−10 Hz), highly resistive and index-matched electrodes composed of organic/Ag-nanowire composites (e.g., Cambrios Clear-Ohm) may resolve electrode diffraction. Diffraction from the splitting features was observed as shown in Figure 6b. Inserting a bit of randomness (noise) into the arrangement of the splitting features eliminates diffraction, as shown in Figure 6c (10% noise/feature pitch ratio). Although diffraction is suppressed in Figure 6c, it also resulted in larger droplets and slower switching speeds as adjacent droplets

dx.doi.org/10.1021/la5008582 | Langmuir 2014, 30, 5357−5362

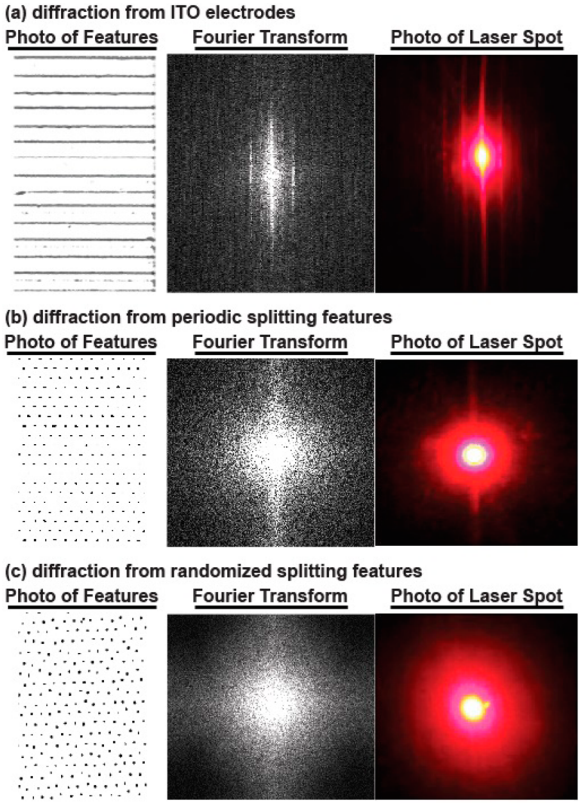


Figure 6. (a) (Left) ITO-patterned substrate image, (middle) resulting DFT image of the ITO pattern, and (right) diffraction from a laser after passing through the patterned ITO. (b) (Left) The patterned splitting features are very periodic (center), resulting in diffraction when performing a DFT and (right) experimentally. (c) (Left) The splitting features are slightly randomized, almost entirely eliminating diffraction (middle) when performing a DFT on the splitting feature image and (right) experimentally.

would in some instances be brought closer and merge together toward the end of the dewetting process. Therefore, an alternate approach is suggested by using gray-scale transmission at the edges of the splitting features. It is well known that gray-scale (nonabrupt cutoff) transmission at the edge of an opaque object significantly suppresses diffraction.[25] Fortunately, the splitting features have a tapered thickness, with a reduction of light-absorbing dye in the splitting feature, and an optimal gray-scale edge may be achievable. Undesirable optical transmission through gray-scale edges in a device's opaque state may not be a major concern as the gray-scale edge is where the splitting feature is very thin and dielectrowetting of ink still occurs over that region because the electrical capacitance is still sufficiently high.

Lastly, it was recognized that the splitting feature pitch can be varied in a single device, and the dynamics of dewetting can be used to impart perceived motion or other visible effects. As shown in the time-lapse images of Figure 7, the area around the arrow is patterned with 0.85 mm pitch hexagonal arrays which dewet in 300 ms. The arrow is then a gradient of less densely patterned splitting features from left to right, forcing the ink into a very visible arrow shape before dewetting after 750 ms on the right side of the arrow which uses the 3.5 mm pitch splitting features. For far-from-eye applications, such as smart windows and transparent signage, this effect might be attractive from an applied perspective (achieve motion or additional information display, with only single voltage/electrode control).

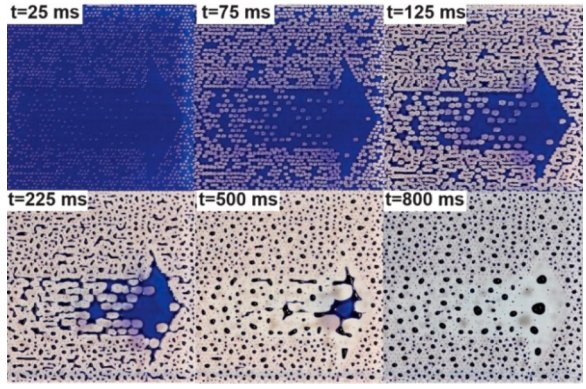


Figure 7. Visual comparison of pitch effect on switching speed. The arrow top has splitting features 3.5 mm apart with a dewetting speed of 750 ms while the surrounding area is patterned with 0.85 mm pitch splitting features which dewet in 300 ms.

SUMMARY AND CONCLUSIONS

This work has provided deeper microfluidic and optical insight into the dielectrowetting superspreading device operation. At first glance, one would argue to scale the device features to as small as those practically possible by commercial fabrication techniques. This would maximize speed, minimize gravity or vibration effects, and eliminate the ability to discern individual dewetted ink droplets visually. However, as seen in the theory and experiments of this work, both microfluidics and optics limit the splitting feature pitch, radius, and size of the dewetted droplets. Smaller features diminish or prevent microfluidic dewetting and depinning and increase optical diffraction, which reduces clarity in the transmissive optical state. Therefore, from an applied perspective, light valves based on dielectrowetting superspreading may find most use in far-from-eye applications (smart windows, larger-area signage). In addition, this work provides further theoretical insight into the operating physics of dielectrowetting superspreading devices and may serve as foundational knowledge for those pursuing research and applications that we have not envisioned or articulated here.

ASSOCIATED CONTENT

Supporting Information

File of Fourier transform code used for image processing. This material is available free of charge via the Internet at http://pubs.acs.org.

AUTHOR INFORMATION

Corresponding Author

*E-mail: heikenjc@ucmail.uc.edu.

Notes

The authors declare no competing financial interest.

ACKNOWLEDGMENTS

We gratefully acknowledge partial support from the National Science Foundation (ECCS 1001146, ECCS 1231668) and from Sun Chemical Corp. We thank Dr. Eric Kreit for subject matter expertise and helpful discussions, Dr. Russ Schwartz (Sun Chemical Corp.) and Mr. Fujino Nobutaka (DIC Corp., Japan) for providing fluid materials, and Collins Ink for the UV-curable ink. We also thank Prof. Glen McHale (Northumbria

University) and Prof. Carl Brown (Nottingham Trent University) for early input and guidance on dielectrowetting superspreading operation.

REFERENCES

(1) Niklasson, G. A.; Granqvist, C. G. Electrochromics for smart windows: thin films of tungsten oxide and nickel oxide, and devices based on these. *J. Mater. Chem.* **2007**, *17* (2), 127−156.
(2) Heikenfeld, J.; et al. Review Paper: A critical review of the present and future prospects for electronic paper. *J. Soc. Inf. Disp.* **2011**, *19* (2), 129−156.
(3) Rauh, R. D. Electrochromic windows: an overview. *Electrochim. Acta* **1999**, *44* (18), 3165−3176.
(4) Granqvist, C. Electrochromic devices. *J. Eur. Ceram. Soc.* **2005**, *25* (12), 2907−2912.
(5) Monk, P.; Mortimer, R. J.; Rosseinsky, D. R. *Electrochromism and Electrochromic Devices*; Cambridge University Press: New York, 2007.
(6) Coates, D. Normal and reverse mode polymer dispersed liquid crystal devices. *Dispersion* **1993**, *14* (2), 94−103.
(7) Vergaz, R.; et al. Modelling and electro-optical testing of suspended particle devices. *Sol. Energy Mater. Sol. Cells* **2008**, *92* (11), 1483−1487.
(8) Zhao, R.; et al. Large area and low power dielectrowetting optical shutter with local deterministic fluid film breakup. *Appl. Phys. Lett.* **2013**, *103* (22), 223510−223514.
(9) Chevalliot, S.; et al. Experimental validation of the invariance of electrowetting contact angle saturation. *J. Adhes. Sci. Technol.* **2012**, *26* (12−17), 1909−1930.
(10) Heikenfeld, J.; et al. Electrofluidic displays using Young−Laplace transposition of brilliant pigment dispersions. *Nat. Photonics* **2009**, *3* (5), 292−296.
(11) Mugele, F.; Baret, J.-C. Electrowetting: from basics to applications. *J. Phys.: Condens. Matter* **2005**, *17* (28), R705−R774.
(12) McHale, G.; et al. Dielectrowetting driven spreading of droplets. *Phys. Rev. Lett.* **2011**, *107* (18), 186101−186104.
(13) McHale, G.; et al. Voltage-induced spreading and superspreading of liquids. *Nat. Commun.* **2013**, *4*, 1605−1611.
(14) Sharma, A.; Ruckenstein, E. Dewetting of solids by the formation of holes in macroscopic liquid films. *J. Colloid Interface Sci.* **1989**, *133* (2), 358−368.
(15) Xu, S.; et al. Color displays based on voltage-stretchable liquid crystal droplet. *J. Dispersion Technol.* **2012**, *8* (6), 336−340.
(16) Taylor, G.; Michael, D. On making holes in a sheet of fluid. *J. Fluid Mech.* **1973**, *58* (04), 625−639.
(17) Varanasi, K. K. Design of Superhydrophobic Surfaces for Optimum Roll-Off and Droplet Impact Resistance. *ASME 2008 International Mechanical Engineering Congress and Exposition*, 2008.
(18) Heikenfeld, J.; Dhindsa, M. Electrowetting on superhydrophobic surfaces: present status and prospects. *J. Adhes. Sci. Technol.* **2008**, *22* (3−4), 319−334.
(19) Ren, H. Dynamics of electro-wetting droplet transport. *Sens. Actuators B: Chem.* **2002**, *87* (1), 201−206.
(20) Kreit, E.; et al. Laplace barriers for electrowetting thresholding and virtual fluid confinement. *Langmuir* **2010**, *26* (23), 18550−18556.
(21) Dhindsa, M.; et al. Virtual electrowetting channels: electronic liquid transport with continuous channel functionality. *Lab Chip* **2010**, *10* (7), 832−836.
(22) Wells, G.; et al. Electrowetting pixels with improved transmittance using dye doped liquid crystals. *Appl. Phys. Lett.* **2013**, *103* (3), 031107−031111.
(23) de Boer, G. B.; et al. Laser diffraction spectrometry: Fraunhofer diffraction versus Mie scattering. *Part. Part. Syst. Charact.* **1987**, *4* (1−4), 14−19.
(24) Huntley, J. An image processing system for the analysis of speckle photographs. *J. Phys. E: Sci. Instrum.* **1986**, *19* (1), 43−49.
(25) Wang, H.; et al. Fighting against diffraction: apodization and near field diffraction structures. *Laser Photon. Rev.* **2012**, *6* (3), 354−392.